SCHOOL OF PHYSICS

FINAL YEAR PROJECT, DISSERTATION OR PHYSICS EDUCATION REPORT

NAME:	**Robert Eskins**
COURSE:	**BSc Physics**
TITLE:	**Nuclear Magnetic Resonance Imaging techniques**
YEAR OF SUBMISSION:	**2021**
SUPERVISOR:	**Stephen Hayden**
NUMBER OF WORDS:	**8384 (Excluding Appendices and Figure Captions)**

School of Physics
Tyndall Avenue
Bristol BS8 1TL

2020/21

DECLARATION

Project Title: Nuclear Magnetic Resonance Imaging Techniques

Declaration

The content in this review has been acquired independently with the use of the sources referenced in the bibliography. All figures have either been recreated or taken from the sources and referenced accordingly.

CERTIFICATION OF OWNERSHIP

Certification of ownership of the copyright in a typescript or manuscript

Dissertation presented as part of, and in accordance with, the requirements for the Final Degree of BSc at the University of Bristol, Faculty of Science.

Author	Robert Eskins
Title	Nuclear Magnetic Resonance Imaging Techniques
Date of submission	27/04/2021

Signed: 

Full name: Robert Eskins

Date:27/04/2021

COVID Implications

Due to COVID restrictions, we were not able to do our intended project. The project that we set out to do was an NMR experiment with paramagnetic ions. Due to lockdown we had to change our project into a literature review in the second term, where we had a reduced time to research the topic of MRI. I would have preferred working on a physical project as it would have motivated me by seeing the physical applications of NMR. This is why I picked a project over a dissertation as I am not at all fond of writing and I find it easier to discuss results that I have obtained as I have a deeper understanding of the physics. I have also found it hard to communicate over email and zoom as it lacks the flow that physical conversations do. This made it hard to discuss ideas and theories with my supervisor. In addition to this, the reduced study space has had an impact on this project as I prefer working in the library or computer room. Overall COVID-19 has had a huge impact on my final year project and I'm disappointed that I couldn't use the labs and do some practical work

Nuclear Magnetic Resonance Imaging Techniques

Robert Jonathan Eskins
School of Physics, University of Bristol

Contents:

Nuclear Magnetic Resonance Imaging Techniques

Robert Jonathan Eskins
School of Physics, University of Bristol

From its first inception into the world of medical physics, Magnetic Resonance Imaging (MRI) has been an essential tool for doctors in identifying disease and abnormalities. However, in order for MRI to produce images for moving anatomy, techniques have been developed to ensure a high temporal resolution. This literature review intends to investigate the fundamental physics behind the imaging, fast imaging pulse sequences and fast data acquisition techniques such as parallel imaging and partial Fourier.

1. Introduction

Nuclear Magnetic Resonance (NMR) is the process in which a nucleus with a non-zero spin in a constant magnetic field is pulsed with a radio wave causing a temporary misalignment with the field. Discovered in 1938 by Isidor Rabi [1], there have been a wide range of applications to further the understanding of physical and chemical properties of atoms [2]. However, one of the most common applications of NMR, is Nuclear Magnetic Resonance Imaging or commonly known as MRI. This involves using the signal generated by NMR, with techniques to spatially localise the signal, to form an image. The benefits of using an MRI over other imaging techniques, is that it does not involve the use of ionising rays such as X-Rays, which are potentially harmful for the body. Due to these advantages, MRI has become an essential tool within hospitals and research centres and has benefited society enormously [3]. The concept of forming an image using NMR was developed in the 1970s and 1980s by many physicists and scientists. The research led separately by Peter Lauterbur and Peter Mansfield lead to a Nobel Prize in 2003 in Medicine and the fundamentals of their research are still used in MRI machines to this day [4].

The first section of the paper will be discussing the fundamental physics of NMR and how a signal can arise when a proton is placed within an external field. This will be vital in understanding how the signal can be generated to form an image. In the second section the fundamentals of how an image can be formed using gradient fields to spatially localise the signal will be discussed. Finally, we can apply this knowledge to understand how techniques have been developed to reduce the scan time and increase the temporal resolution. This is of great interest due to three reasons. The first being that if the scan time is reduced, the patient will have a less stressful experience and will lead to less motion artifacts in the image [5]. The second reason, is that many of the magnets that are used commercially, have to be cooled by liquid helium in order to achieve superconductivity. This will mean as the demand for MRI scans increases, the demand for helium increases and hence the price increases [6]. By reducing the scan time, the cost of running an MRI machine will be reduced and potentially be more accessible for lower income countries. Consequently, more people will be able to be scanned and potentially save lives by identifying disease. The final reason for reducing an MRI scan time will be to reduce it down to a level where you can image moving anatomy such as the heart and respiratory motion [7].

In MRI, a matrix known as k-space is filled with data and used to form an image. The acquisition time is directly related to how this matrix is filled. I have identified three ways that the acquisition time can be reduced. The first is collecting more data in a set period of time which is used by the sequences known as Fast spin echo and Echo planar imaging. The second is reducing the set period of time, and hence more data can be taken. This is utilised by Fast Gradient echo sequences. The third is under sampling the k-space and using parallel imaging techniques to reconstruct the matrix or image [8]. All of these techniques will be discussed in this review, laying down the fundamentals and the applications.

2. Pulsed Nuclear Magnetic Resonance

2.1 Nuclear Magnetic Resonance

2.1.1 Magnetic Properties of Nuclei

Nuclei that have an overall spin quantum number, will possess an angular momentum. This is given by the relation,

$$\boldsymbol{J} = \hbar\, \boldsymbol{I} \qquad \{1\}$$

where $\hbar$ is the reduced planks constant, **I** is the spin of the nucleus and $\boldsymbol{J}$ is the angular momentum. The measurable values of the angular momentum in an arbitrary direction (taken to be the z-axis) can take values from $\hbar I$, $\hbar(\mathrm{I}-1)$,…,- $\hbar(I-1)$**,-** $\hbar I$. Using this, one can calculate the magnetic moment of the nuclei with a given angular momentum to be,

$$\boldsymbol{\mu} = \gamma \boldsymbol{J} \qquad \{2\}$$

where $\boldsymbol{\mu}$ is the magnetic moment and γ is the gyromagnetic ratio which is unique to the type of nucleus. From Equation (1) and (2), it is evident that in order to have a magnetic moment, the nucleus will have to have an overall spin quantum number. There are many nuclei that satisfy this requirement, however, in MRI, we utilise the natural abundance of hydrogen within the body. The hydrogen nucleus is the simplest nuclei in the periodic table and consists of one proton. As a result, the nucleus has total spin of 1/2, resulting in two magnetic moment states in an arbitrary direction (known as proton NMR) [9].

2.1.2 Quantum Interpretation

In Quantum Mechanics, the Hamiltonian for a spin ½ particle in an external magnetic field (**B**), is given by,

$$\mathcal{H} = -\boldsymbol{\mu} \cdot \boldsymbol{B} \qquad \{3\}$$

where the magnetic moment for a proton in the direction of the field is given by $\pm\mu = \frac{1}{2}\gamma\hbar$ (from Equation (1)). From this, the discrete energy eigenvalues of the Hamiltonian are given by,

$$E_+ = -\frac{1}{2}\gamma\hbar B \quad ; \quad E_- = \frac{1}{2}\gamma\hbar \mathrm{B} \qquad \{4\}$$

where B is the magnitude of the magnetic field. The two energy levels correspond to a magnetic moment that is parallel with the field (E_+) and one which is anti-parallel to the field (E_-). As shown, the effect of the magnetic field removes the degeneracy in energy levels. From this, we can derive the energy difference between the energy levels as $\Delta E = \hbar\varpi_0 = \gamma\hbar B$. With a simple rearrangement we can derive the resonance condition,

$$\varpi_0 = \gamma B \qquad \{5\}$$

where ϖ_0 is known as the Larmor frequency [10]. This process is summarised in Figure 1. Furthermore, the distribution of the spin states in the external magnetic field are distributed according to the Boltzmann distribution,

$$\frac{N_\uparrow}{N_\downarrow} = e^{\frac{-\Delta E}{k_B T}} \qquad \{6\}$$

where $N_\uparrow$ is the spin density in the direction of the field,$N_\downarrow$ is the spin density anti parallel to the field, T is the temperature of the sample and $k_B$is the Boltzmann constant [11]. The magnetic moment state parallel to the field is energetically more favourable, leading to an excess of magnetic moments in the direction of the field. This will lead to an overall magnetisation in the direction of the field, which is defined as,

$$M_0 \approx N\frac{\mu^2 B}{k_B T} \quad \{7\}$$

where N is the total number of nuclei per unit volume and M_0 is the magnetisation per unit volume. In order to promote protons into the higher energy state, a radio frequency (RF) pulse is applied with an angular frequency equal to the Larmor frequency. This will mean that the pulse will give exactly ΔE to the proton and will change to the higher energy state. Thus, by adding a RF pulse, the population of energy states change and hence the overall magnetisation will change.

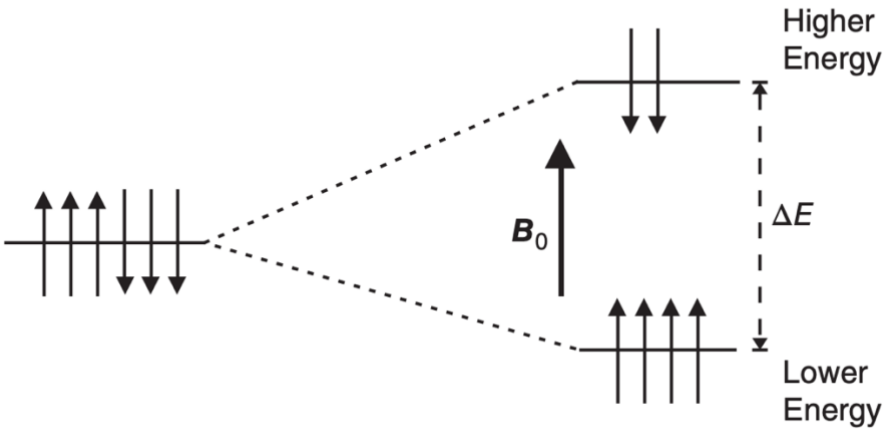

Figure 1*. Energy level splitting for a proton under an external magnetic field B_0. Arrows represent the direction of the magnetic moment. The top row on the right-hand side represents the higher energy level, whereas the bottom row represents the lower energy level. As shown (at T≠ 0) there is an excess of states parallel to the applied field. Taken from* [11].

2.1.3 Classical Interpretation

The application of the magnetic field has removed the degeneracy of the magnetic moment states, and the time evolution of the magnet moment can now be modelled classically. In the Classical Interpretation, the nuclei act as microscopic bar magnets, and under an external magnetic field will experience a torque. This leads to the classical equation, given by,

$$\boldsymbol{\mu} \times \boldsymbol{B} = \frac{1}{\gamma}\frac{d\boldsymbol{\mu}}{dt} \quad \{8\}$$

where $\frac{d\boldsymbol{\mu}}{dt}$ is the change in magnetic moment with time. From this equation, the nuclei magnetic moment will process around the constant external magnetic field at a set frequency. The rate of precession is equal to the Larmor frequency given in Equation (5), showing the overlap between the quantum and classical approach. An analogy of this would be a spinning top in a gravitational field. Due to the vast number of nuclei in the sample with random phases between them, the transverse magnetisation will cancel, and the overall magnetisation will be in the direction of the field. This interpretation is shown in Figure 2 [12].

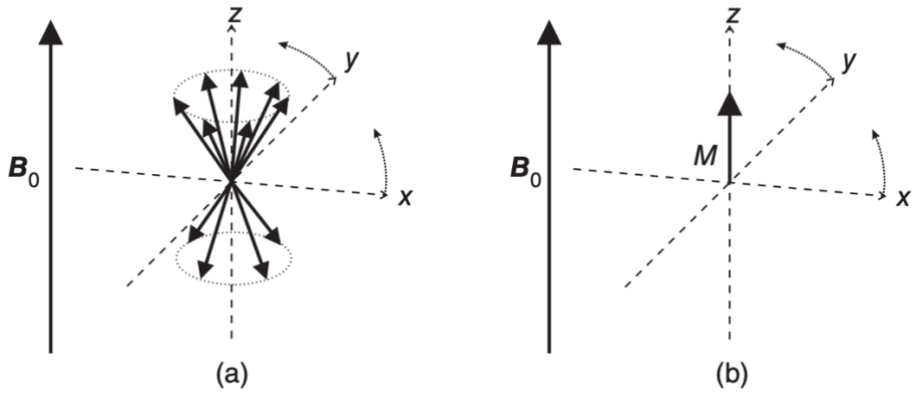

Figure 2. *Classical interpretation of spin alignment in an external field. (a) Individual magnetic moments processing around the external field. (b)The individual nuclei have random phases, and as a result the x-y magnetisation will cancel leading to an overall magnetisation in the z direction. Taken from [11].*

The RF pulse is now seen as a rotating field which rotates at a defined angular frequency ϖ. By defining the static magnetic field in the z direction, the effective magnetic field in a rotating frame is given by,

$$B_{eff} = B_1\hat{\imath}^* + (B_z - \frac{\varpi}{\gamma})\hat{k}^* \quad \{9\}$$

where B_1 is the strength of the pulse, ϖ is the angular frequency and B_z is the constant magnetic field. With the angular frequency of the RF pulse set at the Larmor frequency, it can be shown that in a rotating frame that it will process around a rotating frame direction $\hat{\imath}^*$, with a precession rate equal to,

$$\frac{d\theta}{dt} = \gamma B_1 \quad \{10\}$$

where $\frac{d\theta}{dt}$ is the rate at which the magnetisation processes around the rotating field (See Appendix A for full classical derivation). From Equation (10), it is evident that the duration and strength of the pulse will affect the angle that is formed. The magnetisation can be rotated by any arbitrary angle, however there are two angles that become particularly useful in MRI. The first is known as a 90° pulse, where the magnetisation is flipped into the x-y plane from the z axis. In a non-rotating reference frame, an individual magnetic moment will be seen to follow a 'corkscrew' pattern through space. It is also important to note that this configuration corresponds to an equal distribution between the energy levels. The second is known as a 180° pulse and flips the magnetisation into the -z direction [13].

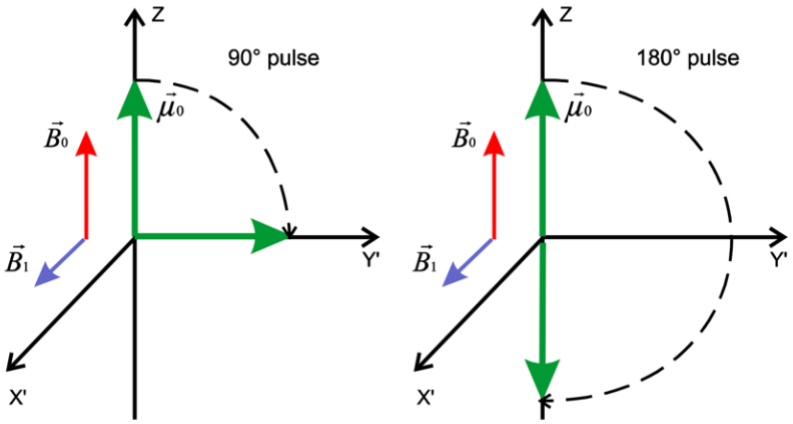

Figure 3. *The effect of a 90° and 180° pulse on the overall magnetisation in a rotating coordinate system. Taken from [9] .*

2.2 Relaxation Mechanisms

2.2.1 Spin-Lattice Relaxation

The RF pulse has caused the magnetisation to rotate by a set angle and as a result the energy levels of the system are in an excited state. The excited distribution is temporary, and the sample will want to return back to thermal equilibrium. This will mean that the overall magnetisation will rotate back and align with the external magnetic field. In order to do so, the nuclei will need to transfer energy to return back to the lower energy level. This is known as spin-lattice relaxation and was first experimentally researched by Felix Bloch in 1940. Bloch described the return to equilibrium by the differential equation [14],

$$\dot{M}_z = -\frac{M_z - M_0}{T_1} \quad \{11\}$$

where T_1 is the spin-lattice relaxation time, M_0 is the equilibrium magnetisation in the z axis and M_z is the magnetisation in the z axis. The solution to this after a 90 ° pulse is given by,

$$M_z = M_0\left(1 - e^{-\frac{t}{T1}}\right) \quad \{12\}$$

The energy that is transferred to return to the lower energy level is given to molecules in the sample (or lattice in solid state NMR). The random motion of the molecules will cause local fluctuating magnetic fields and when the frequency is close or at the Larmor frequency, energy can be transferred. The parameter that governs the random tumbling is known as the correlation time τ_c. This can have a wide range of forms and this is why the environment that the protons reside in, yield different relaxation times [15].

2.2.2 Spin-Spin Relaxation

The RF pulse will not only cause the overall magnetisation to change angle but will cause the nuclei to process coherently. This will lead to an overall magnetisation in the x-y plane that rotates in a sinusoidal fashion in a fixed frame of reference. This coherence does not remain, and the magnetisation in the x-y plane will decrease. The differential that governs how the magnetisation in the x-y plane will change with time is given by,

$$\dot{M}_{xy} = -\frac{M_{xy}}{T_2^*} \quad \{13\}$$

where ${T_2}^*$ is the spin-spin relaxation and M_{xy} is the magnetisation in the rotating transverse plane. For a 90° pulse the magnetisation will decay with the following exponential,

$$M_{xy} = M_0 e^{\frac{-t}{T_2*}} \quad \{14\}$$

The spin-spin relaxation has two components resulting in an overall relaxation time. The first is due to the field inhomogeneities of the constant magnetic field, this will mean that spatially the Larmor frequency will vary. Over time the nuclei will develop a phase change due to this and will lead to a reduction in the magnetisation. The second is due to spin- spin relaxation processes, this is due to many factors which are not time dependent and occur randomly. The overall spin-spin relaxation time is described as,

$$\frac{1}{T2^*} = \frac{1}{T2'} + \frac{1}{T2} \quad \{15\}$$

where $T2'$ is the time dependent relaxation time and $T2$ is the time independent non reversible spin-spin interaction relaxation rate [16].

2.3 Hahn's Spin Echo

In 1950, Erwin Hahn devised the first spin echo pulse sequence [17]. The sequence consisted of a 90° pulse that rotated the magnetisation into the transverse (x-y) plane. The spins were allowed to accumulate a phase difference for a set period of time, then a 180° pulse was then applied. This had the effect of nulling the effects of spin-spin relaxation by field inhomogeneities, as any phases created are reversed by the pulse. This in turn refocuses the signal and forms an Echo, known as a spin echo. The effect on the individual processing spins is shown in a rotating frame of reference (at the Larmor frequency) in Figure 4 [18].

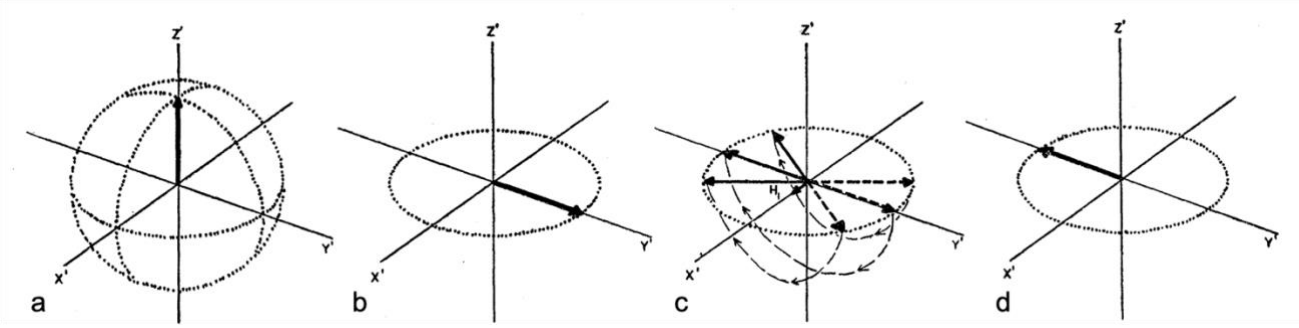

Figure 4. *A spin echo sequence on the individual processing spins in rotating frame of reference (rotating at the Larmor frequency). Arrows indicating the magnetic moment vectors. (a) Equilibrium magnetisation in the direction of the field, (b) 90° pulse, rotating the magnetisation to the transverse plane, (c) Phase accumulation followed by a 180° pulse, (d) Refocusing the signal in an Echo. Taken from [18].*

This process is also shown as a pulse sequence in Figure 5, alongside the signal that is produced in the transverse plane. As shown, the signal created from the 90° pulse quickly decays due to T2* effects. This is known as a Free Induction decay (FID). The 180° pulse creates an echo which has a reduced intensity due to T2 decay. Hence a train of echoes will have intensities that follow an envelope of T2 decay. The signal is detected by a receiver coil in the transverse plane and is detected due to Faraday's law. As the magnetisation sweeps past the receiver, the change in magnetisation induces a current in the coil.

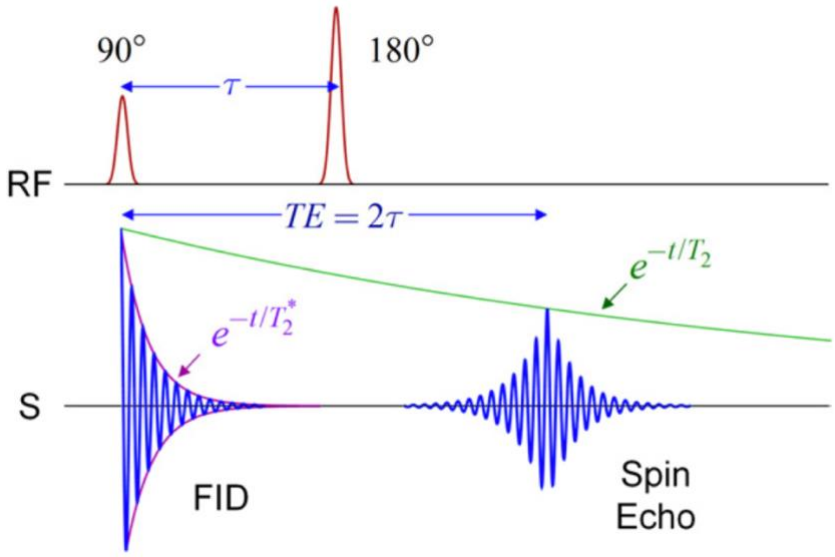

Figure 5. *The spin-echo pulse sequence founded by Hahn in 1950. The sequence consists of a 90° pulse followed by a 180° pulse. The signal is shown by S, indicating the FID and the spin echo formation. TE is the time at which the echo occurs. Taken from [25].*

3. Magnetic Resonance Imaging

3.1 Early Developments of Imaging

In 1971, Damian Raymond discovered that protons in different tissues within rats would produce different relaxation times. Furthermore, he found that tumours would produce longer T1 and T2 relaxation times to healthy tissues [19]. This was significant as you could distinguish the type of tissue based on the relaxation time. After this discovery, the idea of spatially localising NMR signals was in the sights of many physicists. One of the first imaging technique was implemented by Peter Lauterbur in 1972, where he was able to image two water capillaries, known as a phantom experiment, using a projection technique. This was done by applying a gradient magnetic field to the main field, creating a spatially dependent Larmor frequency (as the Larmor frequency depends on the field the proton feels). The signal received would then be a combination of the frequencies. With the use of a Fourier transform the frequencies can be recovered along with the amplitude. With the knowledge of how the frequencies are spatially dependent, an intensity profile can be formed. By rotating the field, an intensity profile will vary and with reconstruction techniques a 2D image can be formed. This process is shown in Figure 6 [20].

After Damian Raymond discovered the difference in relaxation times in tissues, he went on to develop his own technique of scanning a sample in 1972. The method that he developed is known as the Field Focused Nuclear Magnetic Resonance (FONAR), which was essentially a sensitive point method. The method involved having an extremely inhomogeneous field which would only be homogenous over one sensitive point. Due to T2* relaxation effects, the signal from the tissue within the inhomogeneous field would quickly decay. As a result, the signal would be generated at the sensitive point. By moving the sample, (changing the position where the sensitive point is) the whole sample can be imaged. FONAR was the first technique to perform a whole-body scan of a human in 1977 [21], however, the duration of the scan took nearly five hours to produce an image. During this time period, there were a vast amount of imaging techniques that were proposed. Unfortunately, methods such as FONAR, were producing images far too slow for the technique to become commercially viable. They would also need intense precision to produce images that medical conclusions could be formed from.

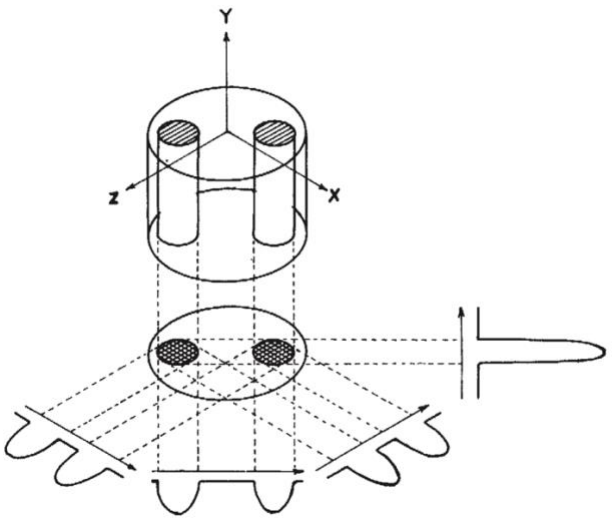

Figure 6. *Lauterbur's projection technique to produce an image of two water capillaries. Rotating the field yields different intensity profiles. Taken from [20].*

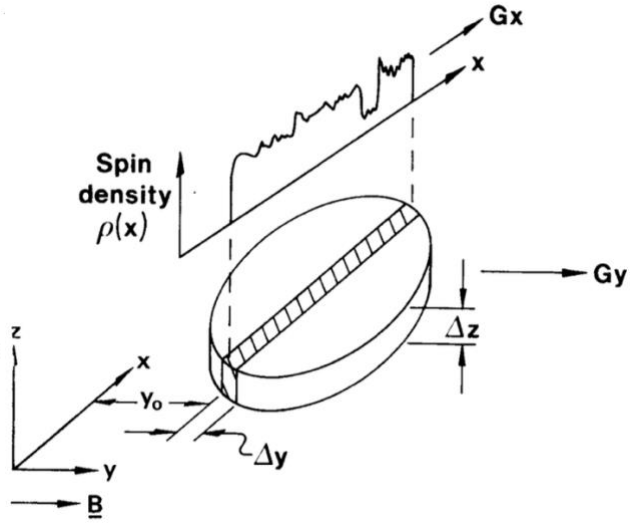

Figure 7. *Line Scan technique developed by Peter Mansfield in 1976. Showing the intensity profile of the line that is being imaged. Apparatus design allowed the use of only two gradients. Taken from [22].*

While many techniques were suggested, the work done by Peter Mansfield in the 1970s was highly significant. The method that he developed is known as the line scanning technique. The use of two gradient fields perpendicular to each other, would essentially localise signal to a strip (or line). This was then used to image

a finger in 1976, which took 23 mins [22]. It is evident that in order to image moving anatomy such as the lungs or heart, techniques in the speed of data collection had to be improved.

3.2 Spatial Localisation

3.2.1 Slice Selective Gradient

The most common way of forming an image in modern MRI machines, is through the application of applying three gradients perpendicular to each other, to spatially localise signal to a slice. This is known as the spin warp technique introduced by Edelstein *et al* in 1980 [23] and any derivation from this technique is fundamentally identical. This practically is implemented through gradient coils placed perpendicular to each other around the patient. The first field gradient is known as the slice selective gradient and is added to the main constant field, which is usually in the z direction. As a result, the Larmor frequency will vary linearly across that dimension, this is given by,

$$\varpi(z) = \gamma\big(B_z + G(z)\big) = \varpi_0 + \gamma G(z) \qquad \{16\}$$

where G is the gradient field applied which varies linearly with position.

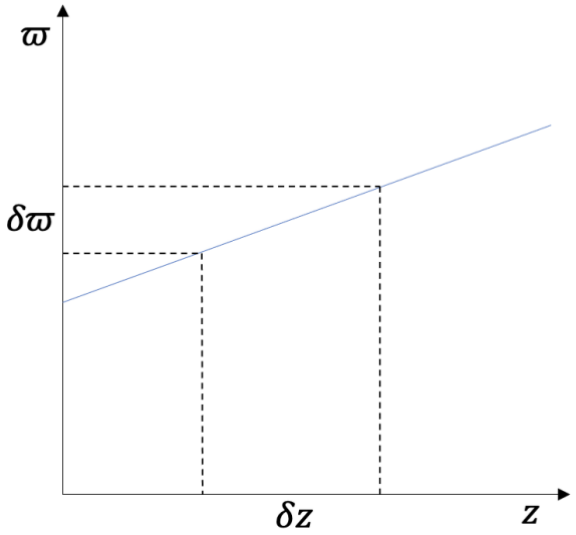

Figure 8. *Larmor frequency as a function of position. Showing how a range of frequencies $\delta\varpi$ excites a slice thickness δz. Adapted from [11].*

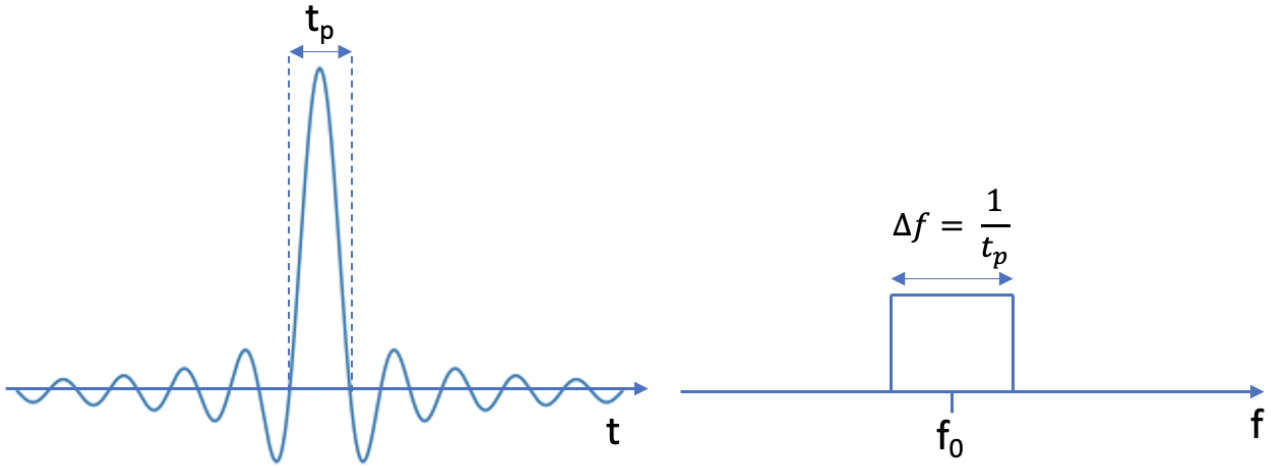

Figure 9*. RF pulse for a SInc waveform and the corresponding Fourier transform. This shows how a range of frequencies(bandwidth) can be excited. Adapted from [24].*

The next step is to apply a tailored radio frequency pulse, to excite a range of frequencies in the gradient field. If the pulse only consisted of one frequency, the slice would not have a depth and the signal to noise ratio (SNR) will be too low to form an image that any conclusions can be formed from. In order to solve this, a range of frequencies needs to be excited. Ideally, this is done using a Sinc function ($\frac{\sin(t)}{t}$) pulse in the time domain. The Fourier transform of this is a top hat function and hence evenly exciting a range of frequencies to give the desired rotation. However, as a Sinc function is infinite in time, more realistic pulses are used such as a Gaussian [24]. Converting this to an angular frequency, it can be shown to excite a slice of sample placed within that field (as shown by Figure 8). From this there are two ways to adjust the thickness of the slice. The first is using a function that excites a larger range of frequencies and the second is using a stronger gradient field. The higher variation in angular frequency will mean that the range of frequencies excited will cover a smaller slice thickness. A thicker slice will provide a higher signal to noise ratio, however if too large the voxel will contain more than one tissue type affecting the image quality.

3.2.2 Localisation within a Slice

In 2D imaging we select the slice that we want to image using the slice selective gradient and then we superimpose another two gradients to spatial localise signal within the slice. Therefore, the gradient field will have the form,

$$B_G(x,y,t) = G_x(t)x + G_y(t)y = \boldsymbol{G}(t)\cdot\boldsymbol{r} \quad \{17\}$$

where $G_x(t)$ is known as the frequency encoding gradient and $G_y(t)$ is known as the phase encoding gradient. The phase encoding gradient is applied for a set period of time and then switched off. During the period when the gradient is on, the nuclei will have a spatially defined Larmor frequency and hence a phase will accumulate. When the gradient is removed the nuclei revert back to the Larmor frequency but with a spatially defined phase. The frequency encoding gradient is applied when a signal is being detected, this spatially defines the signal in the other dimension by the frequency. This is fundamentally how the signal can be localised, however with the use of k-space, this process can be formalised for any combination of applied gradients [25].

3.3 Imaging using Spin-Echo's

3.3.1 K-Space

If we consider a sample where the slice selective gradient has localised the signal to a slice. A single nucleus within the slice will produce a signal equal to,

$$S(t) = Aexp[i(\varpi_0 t + \phi_{acc})] \quad \{18\}$$

where ϕ_{acc} is a phase offset due to its position in the sample and A is a magnetisation constant. We have also made the assumption that the signal will not decay (ignored relaxation effects). For the whole slice, the signal will be due to all the contributions of the nuclei. Hence, the signal becomes,

$$S(t) = A\iint \rho(x,y)\exp[i(\varpi_0 t + \phi_{acc})]dxdy \quad \{19\}$$

where $\rho(x,y)$ is the proton density at a particular location in the slice. After a 90° pulse the phases of the nuclei phases will be identical, and the signal will be at a maximum. With the application of gradients, the phase will depend on the position that the nucleus is within the field. The accumulated phase due to the gradients can be written as [25],

$$\phi_{acc}(\boldsymbol{r},t) = \gamma\left[\int_0^t \boldsymbol{G}(t)dt\right]\cdot\boldsymbol{r} \quad \{20\}$$

After demodulation, the factor $Ae^{-i\varpi_0 t}$ can be removed. Hence the signal can be written as,

$$S(t_x, t_y) = \int\int \rho(x,y) exp\left[i\gamma \int_0^{t_x} G_x(t)xdt + i\gamma \int_0^{t_y} G_y(t)ydt\right] dxdy \quad \{21\}$$

where $S(t_x,t_y)$ is the signal that depends on the time that the gradient fields are applied for [26]. Using this we can introduce a variable known as a spatial frequency(k), this is defined by,

$$k_{x,y} = \frac{\gamma}{2\pi} \int_0^{t_{x,y}} G_{x,y}(t)dt \quad \{22\}$$

With the introduction of this new variable k (See Appendix B for more detail about spatial frequencies), Equation (21) will become,

$$S(k_x, k_y) = \int\int \rho\,(x,y) exp\left[2\pi i(k_x x + k_y y)\right] dxdy \quad \{23\}$$

where $S(k_x, k_y)$ is the signal dependent on the x,y spatial frequencies. Mathematically the signal and the proton density can be recognised as a Fourier pair. Thus, the proton density function $\rho(x,y)$ can be found by acquiring the k-space data and taking the two-dimensional Fourier transform,

$$\rho(x,y) = FT[S(k_x, k_y)] \quad \{24\}$$

Mathematically we can consider the effect of a 180° pulse on the phases of the nuclei precession. As stated previously, the 180° pulse inverts all phases of the nuclei. This can be seen as the complex conjugate of the signal acquired. This is shown by [9],

$$S^*(k_x, k_y) = \int\int \rho\,(x,y) exp\left[2\pi i(-k_x x - k_y y)\right] dxdy = S(-k_x, -k_y) \quad \{25\}$$

and this becomes useful when considering K-space trajectories. In practice the signal acquired will not be solely based on the proton density and relaxation processes will alter the signal. This will mean the proton density function will be an effective function, encapsulating all the processes that change the signal strength.

3.3.2 Conventional Spin-Echo Sequence

With the introduction of spatial frequencies, we can now move onto how the data is collect for the k-space. The data collection is done through a timing sequence known as a pulse sequence. This tells us how the RF pulses and gradients are applied. The simplest pulse sequence is a conventional Spin Echo sequence and is fundamentally the same as the Hahn echo, however adjusted by gradient fields to spatially localise the signal. The pulse sequence is shown in Figure 10 and corresponds to the k-space trajectory in Figure 11. The first step is to excite the slice that you want to image, as discussed previously this is done by the slice selective gradient. This is followed by negative rephasing gradient, in order to reduce signal loss due slice dephasing. This is common to all 2D imaging sequences and will be assumed from this point onwards. Now that the slice is excited, we need to apply gradients to localise the signal. The phase encoding gradient is applied for a set period of time, and with the use of Equation (22), this gives us a definite spatial frequency in the y axis. This is given by,

$$k_y = \frac{\gamma}{2\pi} G_y \tau \quad \{26\}$$

where G_y is assumed to be constant and τ is the duration the phase encoding is applied for. This effectively selects the row in k-space that you want to sample. The frequency encoding is also applied simultaneously in the same manner, so that we end up on the edge of k-space at the maximum spatial frequency in the x direction. The 180° pulse is applied, which flips all phases in the slice and traverses across the k-space to the opposite side. Finally, the echo is sampled in the presents of the frequency encoding (or commonly referred

to as the readout gradient), filling out the row of k-space with the amplitude of the signal[1]. Due to the rephasing of the frequency gradient, the signal is at a maximum at the centre of the echo. The generalised signal equation in Equation (21) can be refined for the spin echo sequence to be,

$$S(t) = \iint \rho(x,y)\exp\left[i\gamma G_x x t + i\gamma G_y y \tau\right]dxdy \quad \{27\}$$

and with the relative assumptions and substitutions ($k_x = i\gamma G_x x t/2\pi$ and $k_y = i\gamma G_y y \tau/2\pi$) can be simplified to Equation (23) [27]. This process is then repeated with different amplitudes of the phase encoding gradient, sampling different rows of the k-space, until the desired matrix is filled. This is then Fourier transformed, and the proton density is assigned a grey scale to visualise the intensity at each location.

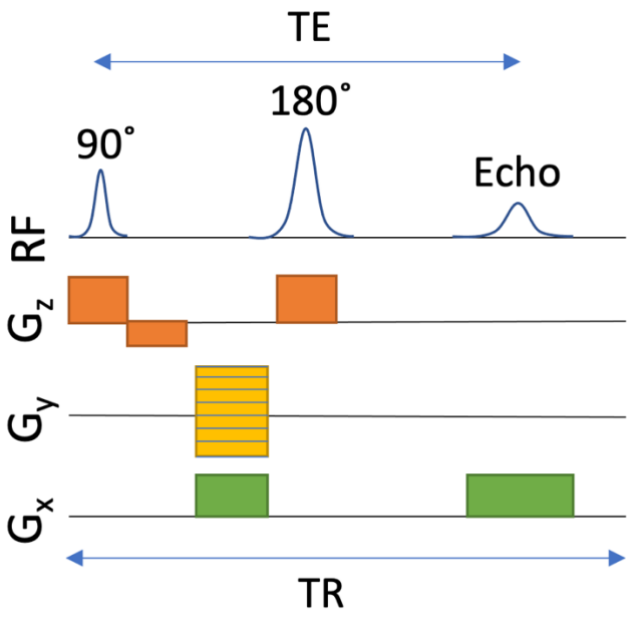

Figure 10. Pulse sequence for a conventional spin echo. G_z is the slice selective gradient, G_y is the phase encoding gradient and G_x is the frequency encoding gradient. The radio frequency pulse is shown in the top row. This consists of a 90° pulse followed by a 180° pulse. Adapted from [27].

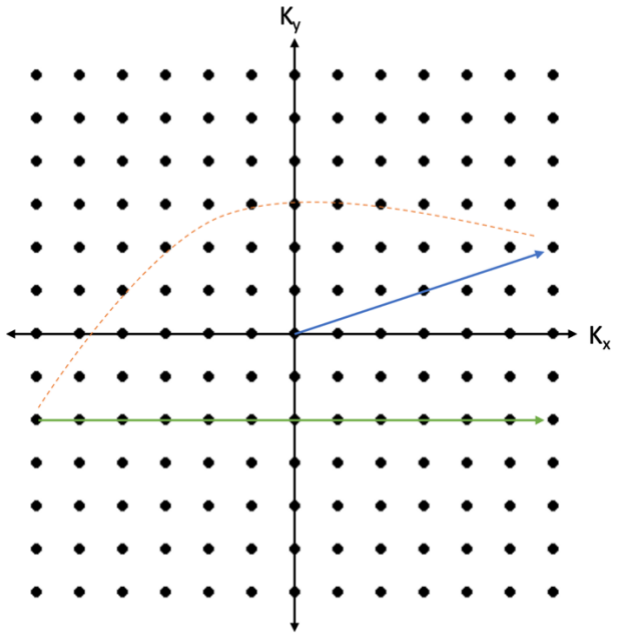

Figure 11. The k-space trajectory for a conventional spin echo sequence. The combination of the G_x and G_y sets a spatial frequency at the edge of k-space represented by the blue line. 180° pulse inverts all phases and then frequency encoding gradient is applied during sampling. Represented by the green line. Adapted from [27].

There are some fundamentally important features of k-space. The first is that the strength of the signal is greatest in the middle of the k-space, this is because the gradient fields are the weakest here. Secondly, the spatial frequencies in the centre give information about the contrast, whereas the higher spatial frequencies give the image the resolution and detail. Finally, a point in k-space is not directly related to a specific point in the image but provides information across the whole image for that spatial frequency. By building up a range of spatial frequencies, which have different weightings, the image can be formed.

[1] In MRI, the complex signal is measured using two coils in an orthogonal arrangement. This gives information about the magnitude and phase of the signal for each point in k-space. Most commonly the magnitude is shown to visually represent the signal and proton density.

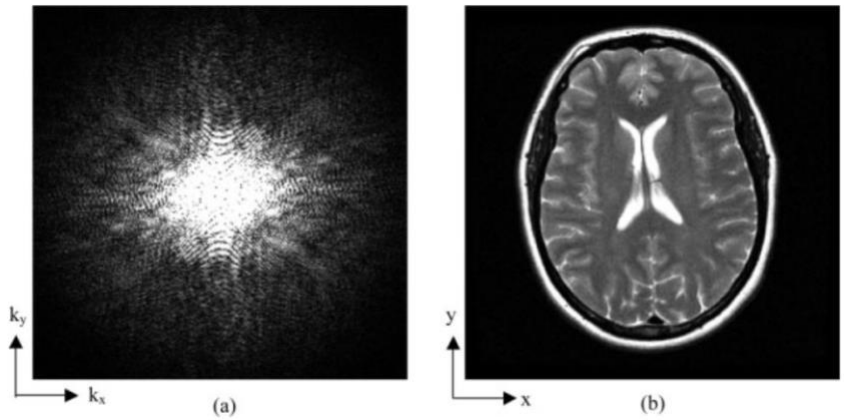

Figure 12. *(a) Example of a typical k-space matrix (b) Fourier transformed image (Magnitude of complex signal is applied on a grey-scale). Taken from [8].*

3.3.3 Resolution

The k-space dimensions directly impact the dimensions in the image space. The field of view (FOV) is defined as the maximum distance that the image covers. This is directly related to the spacing of the k-space and is given by,

$$FOV_x = \frac{1}{\Delta k_x} \; ; \; FOV_y = \frac{1}{\Delta k_y} \quad \{28\}$$

where Δk_x is determined by how fast the signal is sampled and Δk_y is determined by the amount of phase encoding steps used. The resolution of image is directly related to maximum spatial frequency that is acquired. This is given by,

$$\Delta x = \frac{1}{2k_{xmax}} \quad ; \quad \Delta y = \frac{1}{2k_{ymax}} \quad \{29\}$$

where $\Delta x, y$ is the spatial resolution [28] . The region in image space with dimensions $\Delta x \times \Delta y$ is known as a pixel or voxel as it has depth due to the slice selection. It is therefore evident that in order to have an image with the desired dimensions, the sampling of the k-space needs to be taken into consideration. In order to sample a high spatial frequency (and hence have a high pixel resolution) using spin echoes, the signal to noise ratio will have to be high. In ultra-high magnetic field of strength 11.7T, a resolution has been reported of 80×80×200μm^3. However, in commercially used MRI scanners (1.5T or 3T), a typical resolution of 1.5 × 1.5 × 4mm^3 can be achieved [29].

3.3.4 Classifications of Images

The overall signal received by each voxel will be dependent on three parameters. Proton density, T1 relaxation and T2 relaxation. The overall signal from a voxel will be a combination of these parameters given by,

$$S = \mathcal{P}(H)(1 - e^{\frac{-TR}{T_1}})e^{\frac{-TE}{T_2^*}} \quad \{30\}$$

where $\mathcal{P}(H)$ is the proton density, TR is the repetition time (time between successive 90° pulses) and TE is the echo time (time between a 90° pulse and the echo). The use of this equation allows us to classify images based on the parameters TE and TR. The first classification is known as a T1 weighted contrast image, this is where TE and TR are short (relative to the tissues being imaged). This has the effect of extenuating the contrast due to spin-lattice relaxation from the different tissues being imaged. If we consider two regions in a sample, if one region has a high T1 time, the magnetisation has not been able to return when the next 90° pulse is applied. This will mean that the signal that is attributed from this tissue will be reduced, leading to a dimer colour in the overall image.

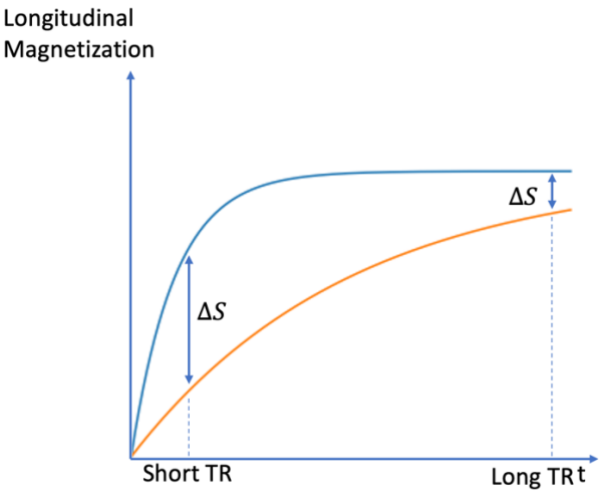

Figure 13. *Longitudinal magnetisation recovery for two different tissues with different T1 relaxation rates. ΔS refers to the signal difference, giving the image contrast. Adapted from [59]*

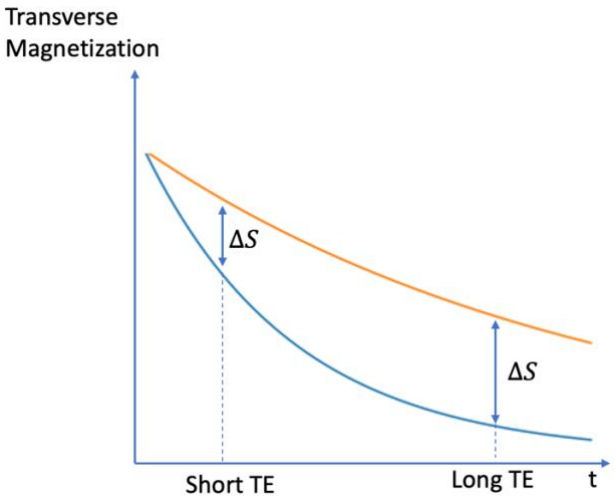

Figure 14. *Transverse magnetisation recovery for two different tissues with different T2 relaxation rates. ΔS refers to the signal difference, giving the image contrast. Adapted from [59]*

The next classification is known as a T2 weighted image, this is where TR and TE are relatively long, leading to contrast between tissues based on their spin-spin relaxation time[2]. Finally, we have the last category of images, this is known as proton-density image. This is achieved by having a long TR and a short TE, leading to the effects of relaxation contrast being minimal. With the use of Equation (30), the classifications of imaging become clear [30]. As shown by Figure 15, the parameters have a substantial effect on the type of image that is formed. Each category has its uses and can be used for different clinical needs.

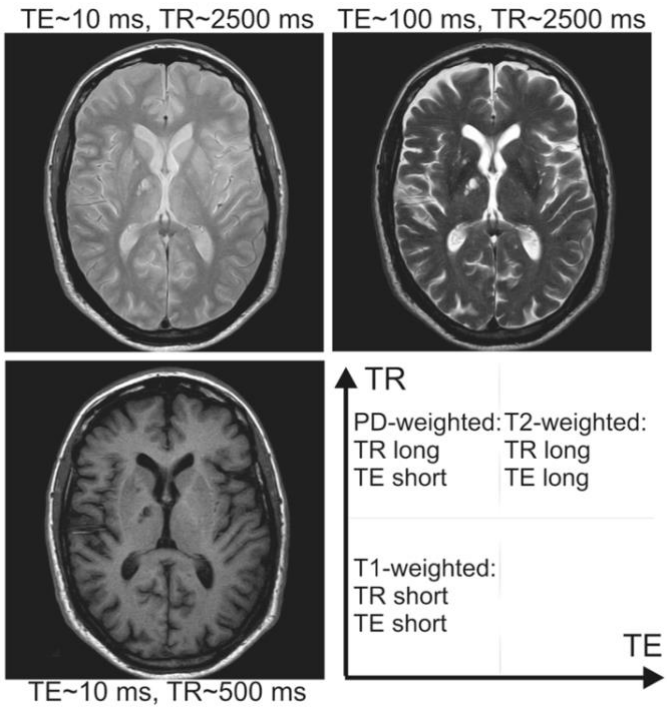

Figure 15. *T1 weighted image, proton density image and T2 weighted image of a brain. Taken from [60].*

[2] Contrast to noise ratio (CNR) between tissues can be defined by the difference in signal from the two tissues over the background signal.

The TR and the number of phase encoding steps will directly result in the total scan time. For example, if the TR= 2500ms to achieve a T2 weighted image and 256 phase encoding steps are needed, this will result in a scan time of around 11 mins. It is evident that this is far too long to image anatomy that is moving. For this reason, it is important to introduce techniques that can reduce this time by manipulating how we collect data through k-space.

4.Fast Imaging Pulse Sequences

4.1 Fast Spin Echo

In conventional SE sequences, the acquisition time is limited by the need for the longitudinal magnetisation to build up to achieve the desired contrast. The Fast Spin Echo (FSE) or Turbo Spin Echo (TSE) uses a train of refocusing 180° pulses within a TR period. Each echo generated is encoded with a different magnitude of phase encoding gradient, filling different rows of k-space in the same TR period. The amount of refocusing pulses in a given TR is known as the Echo Train Length (ETL) and as a result the acquisition time is reduced by a factor of ETL [24]. For the most extreme cases, the ETL can be increased to produce an image in a single shot. As T2 decay occurs, the signal produce at the later echoes will be unevenly weighted and therefore there will be an effective TE (TE_{eff}). This is defined as the time taken to the smallest phase encoding gradient, as this gives the most information about the contrast of the image. The first pulse sequence to be introduced using this method was RARE (Rapid Acquisition with Relaxation Enhancement) and was introduced by Hennig in 1986 [31]. Using the FSE, an image of the brain could be produced in under 2 mins. As shown by Figure 17, with the RARE sequence the images produced are vastly different. The single shot method is vastly different from the conventional SE; however, the lesion is more visible as the bright sections. In comparison, when a 16 shot image is used, the contrast is less but the detail in the rest of the brain is more visible. Due to greater contrast, the sequence can diagnose lesions more accurately.

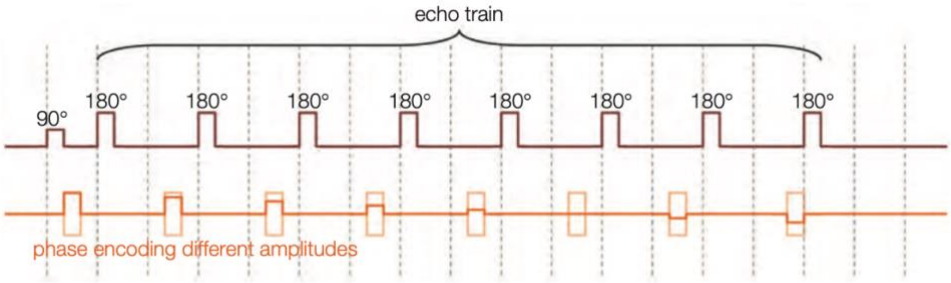

Figure 16. *Fast Spin Echo sequence showing a train of 180° pulses with different phase encoding gradients. The slice selective gradient is applied when a pulse is applied, and the frequency encoding gradient is applied when sampling an echo. Taken from* [24].

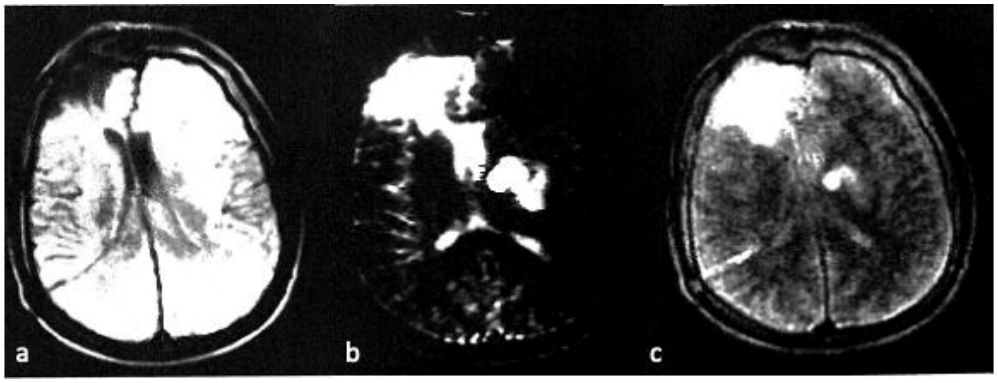

Figure 17. *(a) Conventional Spin Echo sequence, (b)single shot RARE image and (c) 16 shot RARE image of a patient with recurrent pituitary adenoma. Conventional imaging had a TR=1800ms and echo readout time of 33ms. Taken from* [31].

4.2 Gradient Echo

In Gradient Echo imaging, the echo is formed in an alternative manner to applying a 180° pulse. This is done by applying a negative gradient, accelerating the effects of dephasing in the FID. Subsequently, the polar opposite field can be applied, rephasing the induced phase difference caused by the dephasing gradient and forming an echo [32](summarised in Figure 18). At the echo peak the net gradient application is zero and the magnitude will be due to T2* effects. The need for a 180° pulse is removed and a reduced flip angle can be used. This will mean that the time required for the longitudinal magnetisation to recover is reduced and more echoes can be sampled with different phase encoding steps. This in turn results in the data for the k-space being acquired in a shorter period of time. The gradient echo sequence can produce images very quickly in relation to the FSE. The shortest practical TR for a spin echo sequence is 200ms, whereas for the gradient echo a TR of 2-5ms can be achieved [33]. The gradient echo pulse sequence is shown in Figure 19 and as shown is identical to the spin echo expect for the application of a 180° pulse. The downside of using a reduced flip angle is that the signal generated from the magnetisation is reduced as the magnetisation is only partially flipped into the transverse plane (as the receiver coil can only detect transverse magnetisation). Additionally, with the removal of the 180° pulse, the field inhomogeneities are not corrected and the image will be a T2* weighted image. This method was first introduced under the name FLASH (Fast Low-Angle Shot) by Axel Haase *et al* [34]. Under this sequence, an image (256x256) was produced within 6s [3].

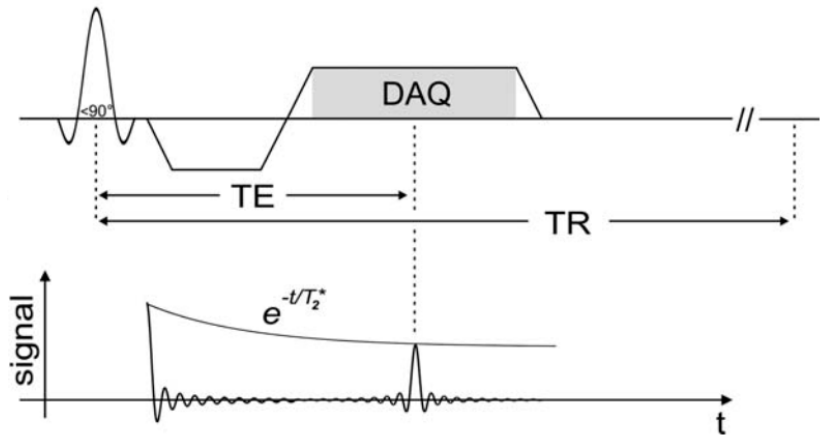

Figure 18. *Gradient Echo Sequence. Top line represents the sequence, collapsed onto one line. Bottom line represents the signal that is present. Taken from* [32].

In addition to the reduced flip angle, TR can be shortened so that it is smaller than average spin-spin relaxation (TR<2T2). This regime is called the Fast Gradient Echo. This will mean that there will be a residual transverse magnetisation and longitudinal magnetisation when the next RF pulse is applied. This leads to a steady state magnetisation that is present when multiple RF pulses are applied. If this can be compensated, it will lead to sequences that are extremely quick. In most sequences this is done by a spoiler gradient, which dephases any residual magnetisation, ready for the next RF pulse [35].

[3] Hard to quantitively compare sequences due to the many parameters that determine the total scan time. Such as the spatial resolution and TR to achieve contrast. However, the scale of time can be compared.

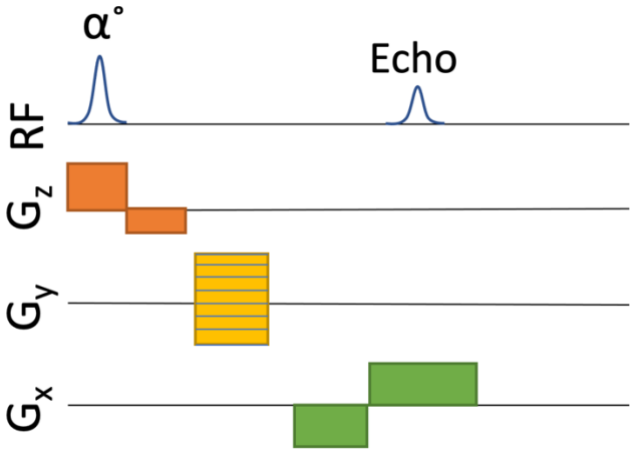

Figure 19. *Gradient Echo Sequence for a flip angle α°. G_z is the slice selective gradient, G_y is the phase encoding gradient and G_x is the frequency encoding gradient. Adapted from* [27].

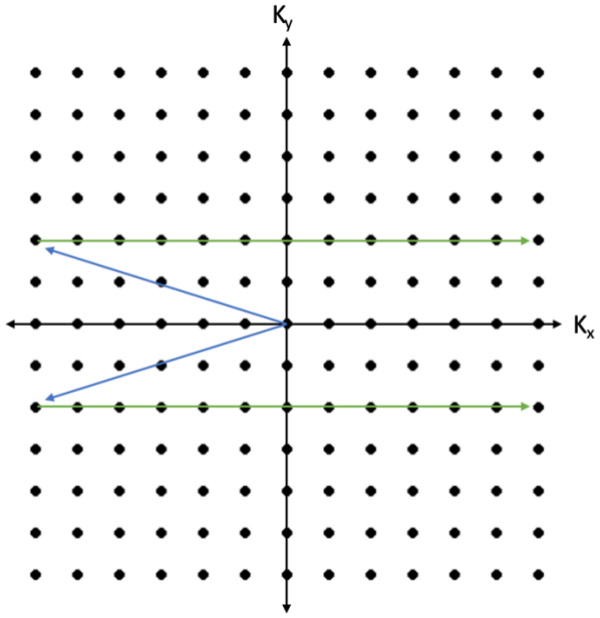

Figure 20. *K-Space trajectory for the Gradient Echo Sequence for two phase encoding steps. Blue line represents the combined effect of the phase encoding and negative frequency encoding. Green represents the frequency encoding during echo sampling.*
Adapted from [27].

4.3 Echo Planar Imaging

Echo Planar imaging (EPI) is a technique that was developed by Peter Mansfield in 1977 [26] and uses a series of alternating gradients to cover k-space in either a single shot or multi shot. As a result, this method can acquire data very fast, on the scale of milliseconds. The sequence can either be achieved by a gradient echo or a spin echo, but the principles of how the k-space is traversed is the same. The first step is to apply a negative gradient in the frequency and phase encoding gradient. This gives a starting point for the sampling and in this case is the bottom left of the k-space. The rows of k-space are then sampled with an alternating frequency encoding gradient with a small phase encoding gradient to transfer between rows in the k-space which partially recover the magnetisation. This results in a train of echo's which has a maximum amplitude value when the middle of k-space is being sampled. As with FSE, there is an TE_{eff} which will define the contrast of the image [36]. This is shown in Figure 21 and 22.

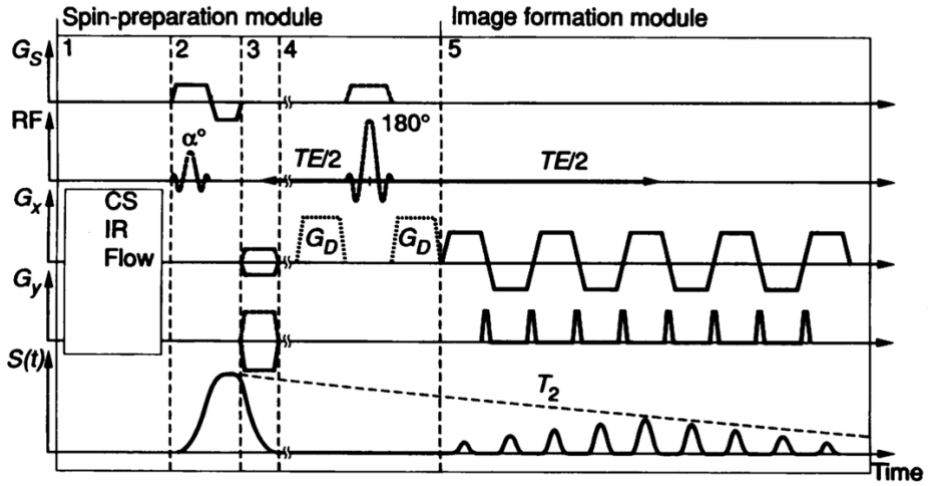

Figure 21. *Pulse Sequence for a spin echo EPI sequence. G_x is the frequency encoding, G_y is the phase encoding and G_s is the slice selective gradient. Taken from* [58].

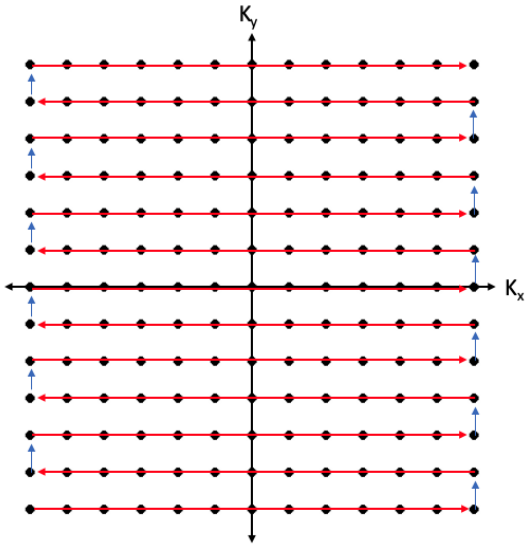

Figure 22. *K – Space Trajectory using the EPI technique. The red lines indicate the frequency encoding gradient, and the blue lines represent the phase encoding gradient. Adapted from* [36].

This was hard to implement due to the rapid change in gradient fields and wasn't fully implemented on a human until 1983, when an infant's heart was imaged. Using this method, an image of the heart could be made within 35msec. Although a great breakthrough for the technique, the resulting image was only 32x32 pixels and had a resolution of 6mm. The image shows lack of quality and shows that an improvement will have to be made to be clinically a success [37]. However, as technology has developed, higher resolution images can be formed due to faster changing gradients and better SNR. Figure 23 shows the difference between a FSE image and an EPI. As shown, due to patient movement there are large motion artifacts, rendering the image useless in diagnoses. The EPI image was taken 5 minutes after and because of its speed, does not suffer from this problem [38]. This is the main advantage of the EPI technique and almost freezes anatomy in time. However, due to signal loss and T2* blurring (only applicable to gradient EPI) the images are not as sharp as the SE corresponding image. Nevertheless, if anatomy such as the heart can be imaged with EPI where SE cannot, the benefits outweigh the negatives.

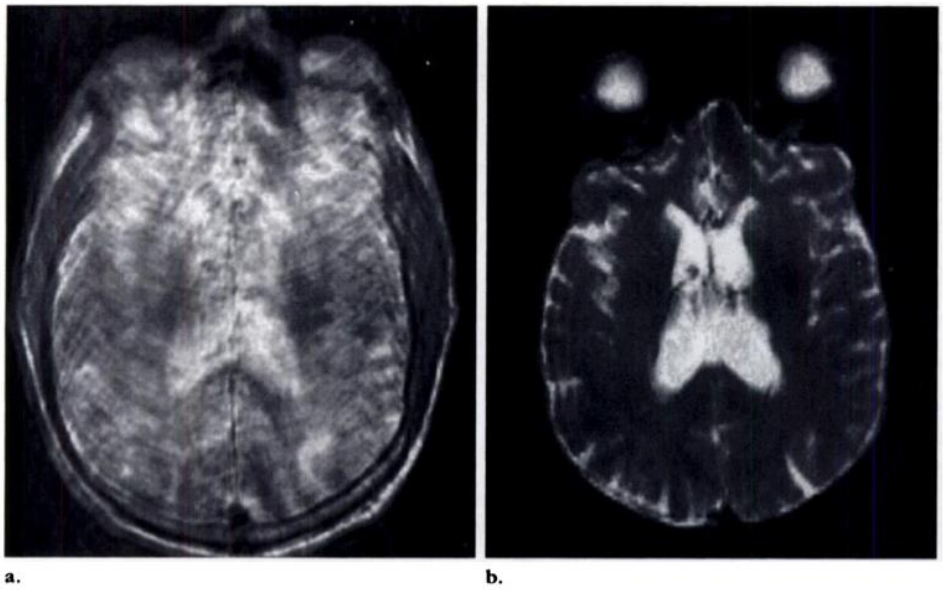

Figure 23. *Images of the brain. (a) FSE T2 weighted image (b) Eco-planar T2 weighted image. FSE shows a large motion artefact. Taken from* [38]

The techniques described to achieve fast imaging all rely on the accuracy of the system. EPI in particular relies on the timings of the gradients to correctly determine the spatial frequency and any slight errors in this will result in incorrect spatial encoding. This is extenuated by the fact that the sequence is performed in a matter of milliseconds, leading to slight imperfections causing great harm to the image. Along with these problems there are instrumental errors resulting from concomitant fields. Concomitant fields are produced when trying to apply a linear field. For example, if you try applying a linear field in the z-axis, there will be non-linear contributions in the x and y direction. As fast imaging sequences have a relatively long readout period, this effect can cause errors in the spatial encoding [39].

4.4 Alternative K-Space Trajectories

In MRI there are a few non-Cartesian methods that differ from collecting spatial frequencies row by row. The first is known as a Spiral k-space and this uses sinusoidal gradient fields to spiral the data collection from the centre. This method was introduced by Ahn *et al* [40], and was introduced to tackle the problem of having a rapidly alternating gradient field in EPI, which at the time, proved difficult with the technology available. The use of an Archimedean spiral will result in a gradient that is easily predictable and easier to apply. This technique is beneficial in cardiac imaging, due to the way the centre of k-space is sampled first. This reduces the effect of flow effects and hence advantageous for this application [41]. Another alternative is known is a radial k-space trajectory, this is achieved by having the Frequency and Phase encoding gradient on during the echo sampling. This means for every data point of the sampled echo; the spatial frequencies will change linearly from the centre of the k-space. This also means that the centre of k-space is more densely filled, leading to more contrast between the images [42].

5. Fast Data Acquisition Techniques

5.1 Half Fourier

Techniques such as the half-Fourier single shot turbo spin echo (HASTE), construct a partial k-space and use the conjugate symmetry of k-space to estimate the remaining k-space lines [43]. As discussed previously, this can be represented by,

$$[S(k_x, k_y)]^* = S(-k_x, -k_y) \quad \{31\}$$

The minimum k-space sampling is a half, and this provides all the necessary information to reconstruct the other half (shown in Figure 24). The phase encoding steps are therefore reduced by half and hence the scan time is reduced by half. This means that HASTE (a fast spin echo sequence) can have an ETL that fits within one TR and hence can be done in a single shot. A study done by Richard Semelka *et al* imaged the abdomen using a T2 weighted HASTE image sequence. The abdomen could be imaged with 15 slices in a duration of 22 seconds (acquiring the data for a single image in less than one second). They also stated that the images were free from breathing, bowel movement or susceptibility artifacts. The technique was highly acclaimed by the research group and they had incorporated it into their imaging protocol [44].

5.2 Parallel Imaging

5.2.1 Under sampling in the Phase Encoding Direction

In parallel imaging (PI) the use of array coils can be utilised to under sample the k-space and used to reform the image after the k-space data has been acquired. The under sampling is done in the phase encoding direction resulting in a reduction in scan time. An example is given in Figure 25 which has an acceleration factor (R) of 2. This means that Δk_y is increased and the hence the FOV_y is reduced by the acceleration factor. The array coil is then used to reconstruct the image in either the image space (SENSE) or the k-space (SMASH). For an individual coil in the array, the positioning of the coil will result in a sensitivity profile. For example, if the coil is placed on the left-hand side of the sample, the signal resulting from the left-hand side of the sample

will be stronger. This can provide more information about how the signal is spatially distributed across the sample [45].

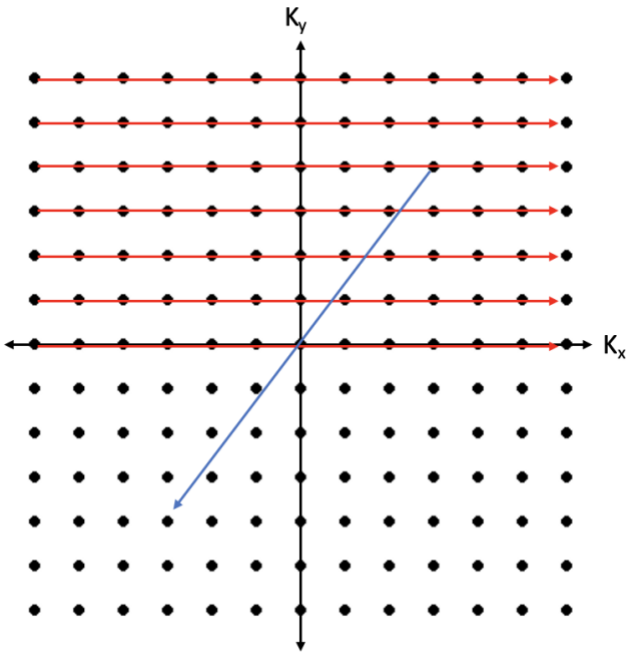

Figure 24. *K-Space reconstruction of a partial k-space. Red lines indicate the k-space points that have been acquired and the blue line shows how a point in the partial k-space relates to an unsampled point based on the conjugate symmetry. Adapted from* [43].

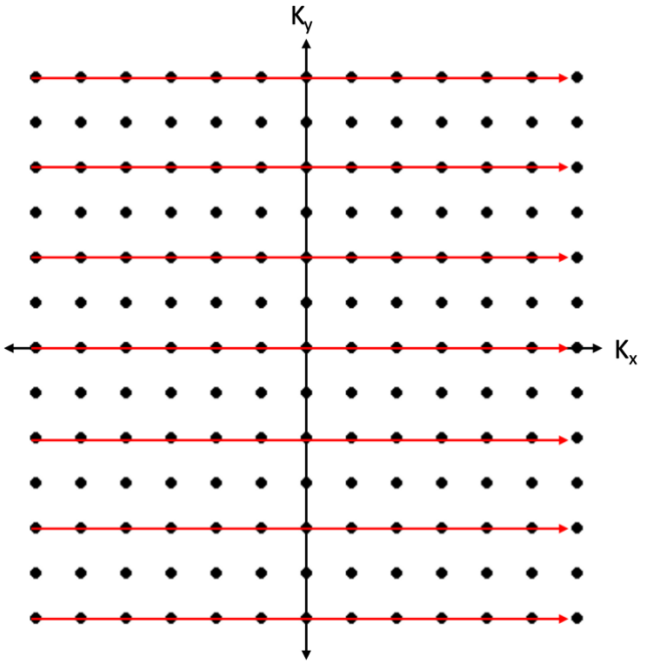

Figure 25. *Under sampling the k-space in the phase encoding direction* (k_y) *by an acceleration factor (R) of 2. Red lines indicate the rows that have been acquired. Adapted from* [46].

5.2.2 SENSE

If the reduced FOV is smaller than the sample being imaged, this will lead to aliasing. This is a process in which nuclei outside the FOV will still contribute to the signal, however, are not correctly encoded and hence the obtained picture has an overlapping effect (as shown by Figure 26). However, this effect can be used to reconstruct the image after the Fourier transform is performed. This is the essence of SENSE and uses the partial images from the coils to reconstruct the full FOV. A pixel in the reduced aliased image, will contain information from multiple pixels in the full FOV image, which will be dependent on the coil sensitivity profile which is made before the measurements. The signal in one pixel at location (x,y) received by the *j'th* coil is given by,

$$I_j(x,y) = C_j(x,y_1)\rho(x,y_1) + C_j(x,y_2)\rho(x,y_2) + \cdots + C_j(x,y_N)\rho(x,y_N) \quad \{32\}$$

where $C_j(x,y)$ is the coil sensitivity at location (x,y) and $\rho(x,y)$ is the proton density at that position. For all coils and all aliased pixels, a linear equation can be found to be,

$$\boldsymbol{I} = \boldsymbol{C} \cdot \boldsymbol{\rho} \quad \{33\}$$

where **C** is the coil sensitivity matrix with dimensions N_c x R. N_c corresponds to the number of coils and R is the number of overlapping pixels. In a situation where the background noise is not accounted for, the generalised solution of this is given by,

$$\boldsymbol{\rho} = (\boldsymbol{C}^H \boldsymbol{C})^{-1} \boldsymbol{C}^H \cdot \boldsymbol{I} \quad \{34\}$$

In a general situation, all pixels can alias, and hence the coil sensitivity matrix becomes very large for reconstruction [46]. This process is depicted in Figure 26 and shows how the desired pixels can be calculated.

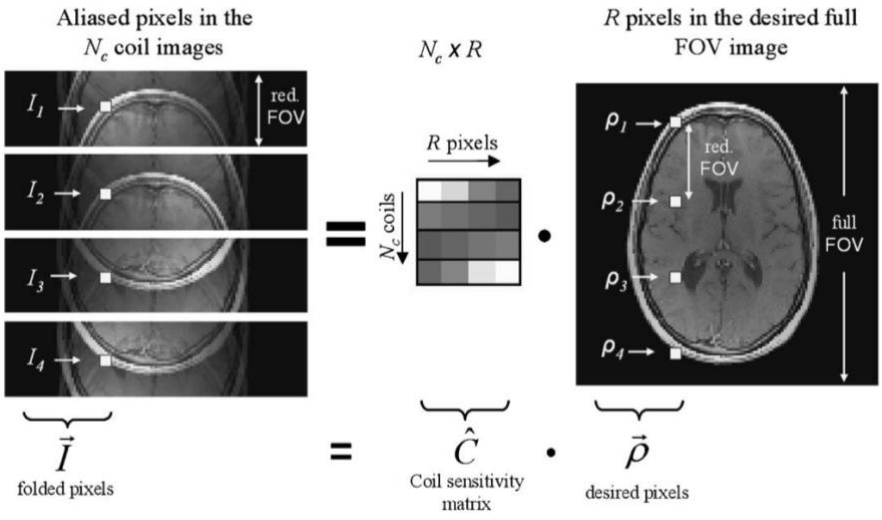

Figure 26. *Pictorial representation of Equation 33 showing how the folded images from the coils can be unfolded, producing a full FOV image. Taken from* [46].

5.2.3 SMASH

SMASH (Simultaneous Acquisition of Spatial Harmonics) is a method that reconstructs the under sampled k-space before the Fourier transform is performed. The signal that is present in a coil from a slice is given by [47](Note: Redefinition of k to move in line with literature on PI),

$$S_j(k_x, k_y) = \iint C_j(x,y)\rho(x,y)\exp\left(i(k_x x + k_y y)\right)dxdy \quad \{35\}$$

where $C_j(x,y)$ is the coil sensitivity of the *j'th* coil. In conventional k-space acquisition, the phase encoding gradient applies a sinusoidal modulation across the sample, from which the signal is detected at different gradient strengths. It is possible to synthesise this effect by weighting the coil sensitivities to achieve this modulation. Figure 28 shows how the manipulation of the weightings of a gaussian sensitive coil can induce a sinusoidal modulation across the slice. This is known as a spatial harmonic. The coil sensitivity to achieve the desired modulation can be calculated to be,

$$C^{comp}(x,y) = \sum_j w_j^m C_j(x,y) = \exp\left(im\Delta k_y y\right) \quad \{36\}$$

where w_j^m is the weighting for each coil for the *mth* harmonic and Δk_y is the desired spacing in the fully reconstructed image ($\Delta k_y = 2\pi/FOV_y$, due to redefinition). Combing Equations (35) and (36), the signal received by the whole array with the desired weighting equals [48],

$$\begin{aligned}\sum_j w_j^m S_j(k_x, k_y) &= \iint \rho(x,y)\exp\left(i(k_x x + k_y y)\right)\exp\left(im\Delta k_y y\right)\, dxdy \\ &= \iint \rho(x,y)\exp\left(ik_x x + i(k_y + m\Delta k_y)y\right)dxdy \\ &= S(k_x, k_y + m\Delta k_y)\end{aligned} \quad \{37\}$$

In summary, by applying the different weightings needed for the spatial harmonics for each coil, it is possible to shift the data by Δk_y. Allowing multiple lines of k-space data to be acquired simultaneously. Figure 27 shows an echo planar imaging sequence that has under sampled the k-space by a factor of 5. Using the

weightings for the required spatial harmonics (m=-2,-1,0,1,2) each shifting the data by a factor of mΔk_y , you can acquire the data for missing k-space rows.

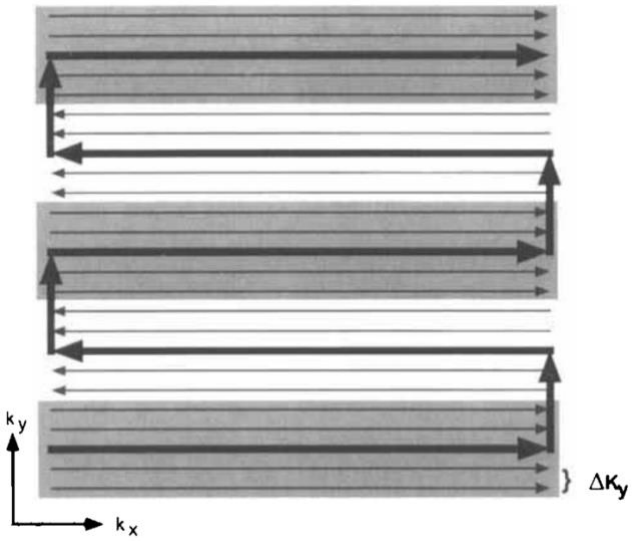

Figure 27. *Echo planar imaging with an acceleration factor of 5. Thick horizontal lines represent the frequency encoding, thick vertical lines represent the phase encoding and thin lines represent the k-space lines that need to be reconstructed. This will correspond to five harmonics, m = -2,-1,0,1,2. Taken from* [48].

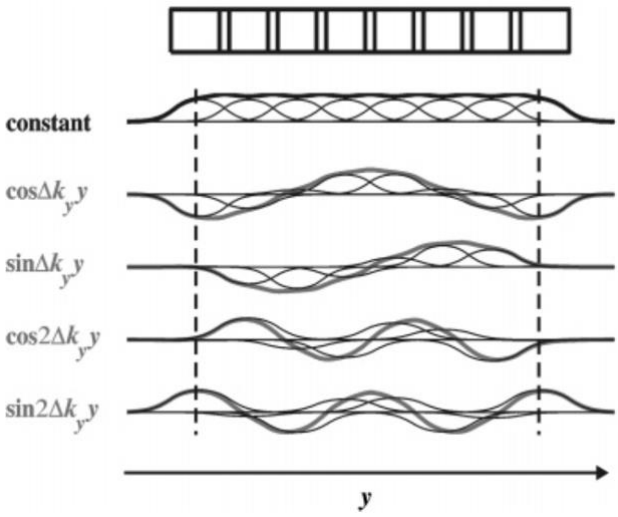

Figure 28. *Example of harmonics using array coils, showing modulations up to the second harmonic. Thin lines represent individual coil sensitivities and solid line represents the overall weighted array sensitivity). Taken from* [48].

Parallel imaging techniques have revolutionised the way that imaging is done. Other than the reduced acquisition time, the main benefit is that it can be combined with any pulse sequence, minimising the need to settle with imaging parameters that might not be beneficial to the user. For example, the echo planar imaging technique will be a T2* weighted image (gradient EPI), however this might not diagnose a problem, like a T1 weighted image might. However, the main drawback of PI is the reduction in the SNR, this can be shown to be inversely proportional to the square root of the acceleration factor (R) [49]. Therefore, the need for larger magnetic fields to boost the SNR is necessary and the general trend of MRI magnets is to achieve greater magnetic strength.

5.3 HASTE with Parallel Imaging

The HASTE sequence can be combined with parallel imaging to further decrease the acquisition time. As shown by Figure 29, the HASTE sequence is used to sample half the k-space and within this, the data is under sampled (smaller phase encoding steps are fully sampled to ensure contrast). The k-space is then reconstructed, and the other half is generated using symmetry. This method was used by Ling Zhang *et al* to image the Carotid Artery and was called PHASTE. This method was used because the standard FSE suffers from motion artifacts and due to the signal loss from later echoes, blurring would be present in the final image [50].

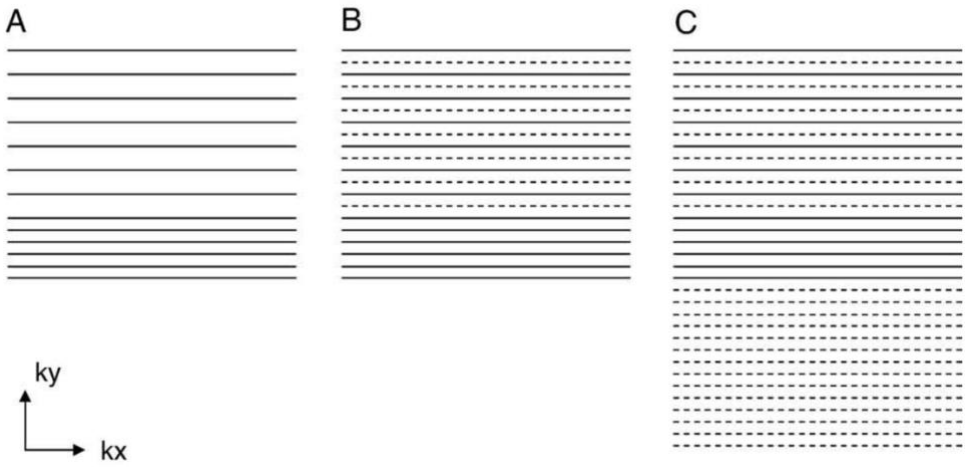

Figure 29. *Diagrammatic representation of how a partial and under sampled k-space is reconstructed for R=2. Solid lines represent acquired data from sampling and dotted represent generated data. (A) The acquired data with under sampling in the phase encoding direction. (B) Reconstructing missing k-space data with parallel imaging. (C) Full k-space reconstruction using the conjunction properties of k-space. Taken from* [50].

This technique has also been known to image the lungs as an alternative to Computed Tomography (CT), eliminating ionising rays. The lungs are difficult to image for many reasons. The first being the motion of the lungs, however, can be overcome with a breath hold. The second is due to a very low proton density, this means that the SNR will be extremely low and by applying a train of spin echoes will be hard to recover for later echoes. Finally, the lungs have a short T2 relaxation time, further increasing the difficulty. However, a study done by Thomas Henzler *et al* showed that the lungs could be imaged under the PHASTE method, and that medical conclusions could be formed from [51].

6.Recent and Future Advancements

More recently, a study done be Martin Uecker *et al* [52] in 2010 showed by using a radial k-space trajectory for the FLASH sequence, they could produce real-time movies of the human heart at a temporal resolution of 20ms. Due to the technical advances of superconductivity, a 3T machine could be used. This is far greater than the magnets used in the early development of MRI. As a result, a flip angle of 8 degrees could be used while maintaining a good SNR. They also used a sophisticated under sampling method that utilises the radial scheme. This shows that the drive for a small temporal resolution is still being constantly reviewed and new techniques being suggested. As many techniques for fast imaging have been established and widely used by many companies in the industry, the idea of fast imaging becomes more complex and relies on the technology. However, with the introduction of deep learning networks, there has been new interest in the applications for MR imaging. The details of deep learning are beyond the scope of this review but give an insight to the progression of fast imaging. The network can be given a subsampled k-space and a fully populated k-space as an output and learn the necessary information to reconstruct the k-space. It has been shown that the network produced by Hyun *et al* [53], could produce an image with a k-space only filled with 29%. This method is highly superior to the Half Fourier technique and combined with a fast-imaging sequence could produce images in real time.

Overall, the fast-imaging techniques described in this paper are dependent on a high SNR. As a result, there has been a drive to achieve higher magnetic field strengths as this will provide a signal that is stronger for the receiver coil to detect. Furthermore, the benefit of reducing the scan time is that 3D imaging becomes more accessible. 3D imaging requires an additional phase encoding step to spatially localise signal in the third plane, further increasing the scan time by a factor of the second phase encoding step. With conventional techniques, this becomes nearly impossible for commercial use. Using the example stated in Section 3.3.4, the conventional spin echo took around 11 mins to produce an image. If you want to extend this to a cubic k-

space, this will take nearly 2 days to complete. In addition to this, a 3D Fourier transform will have to be used, increasing the data processing time. However, with the introduction of fast imaging techniques and parallel imaging, this can be achieved. For example, a 3D spoiled gradient echo sequence has been known to be able to image the hepatobiliary system within a breath hold [54]. Other than increased data collection speed, there are many reasons why a company would want to use a higher field MRI machine. One would be increasing the resolution of an image as more phase encoding steps could be implemented in both the phase and frequency encoding gradient. This would mean that potentially, diseases could be identified earlier and could save lives as a result [55]. As the field of MRI progresses, fast-imaging techniques are only limited by the technology that implement them. Naturally as technology advances, we can expect an increase in resolution, and scan speed. If these factors can be improved, MRI may supplant other imaging techniques.

7.Concluding Remarks

This review has explained the underlying physical principles behind the image creation from the magnetic properties of a proton to the pixel that is present in an image. Using the formalism of k-space, fast imaging techniques could be described by the trajectories through the k-space. This includes fast imaging sequences such as FLASH, RARE and EPI and parallel imaging techniques such as HASTE, SENSE and SMASH. Fundamentally the scan time of an MRI is limited by the need to apply multiple phase encoding steps. Ultimately a technique that could remove this would revolutionise the MRI process, however, is not apparent or commonly used. I think this could become more possible with the use of parallel imaging, rather than the use of fast pulse sequences and I believe reconstruction techniques will be the future of MRI.

8.Acknowlegements

I would like to thank Professor Stephen Hayden for his continually support and knowledge of NMR. I would like to also thank the authors of the papers referenced for the information.

9.Appendices

Appendix A: Classical Description of NMR

The classical motion of a nuclei within an external magnetic field (B) can be modelled classically by,

$$\frac{d\boldsymbol{M}}{dt} = \gamma \boldsymbol{M} \times \boldsymbol{B} \quad \{A.1\}$$

where **M** is the magnetisation of the nuclei. Then if we apply a rotating field which has the form,

$$\boldsymbol{B}(t) = B_1 \cos(\varpi t)\boldsymbol{i} + B_1 \sin(\varpi t)\boldsymbol{j} + B_z \boldsymbol{k} \quad \{A.2\}$$

where ϖ is the angular frequency of the rotating field. If we move to a rotating frame of reference that is rotating at the angular frequency of the rotating field, the rotating field will appear stationary. Due to the rotating frame of reference, there will now be a fictious field along the z direction. Hence,

$$B_{eff} = B_1 \hat{\imath}^* + (B_0 - \frac{\varpi}{\gamma})\hat{k}^* \quad \{A.3\}$$

where $\hat{\imath}^*$and $\hat{k}^*$ are rotating frame coordinates. Using this, the change in magnetisation in a rotating frame is,

$$\frac{d\boldsymbol{M}}{dt} = \gamma \boldsymbol{M} \times \boldsymbol{B_{eff}} \quad \{A.4\}$$

Now if we set the rotating field to the Larmor frequency, such that $\varpi = \varpi_0 = \gamma B_0$, the $\hat{k}^*$ component of the field disappears. As a result, the magnetisation begins to process around the rotating magnetic field. This is shown by,

$$\frac{d\theta}{dt} = \gamma B_1 \quad \{A.5\}$$

This is shown in Figure 3 in section 2.1.4.

Appendix B: Physical Interpretation of Spatial Frequencies

If we consider a one-dimensional line of processioning nuclei, with the application of a gradient magnetic field and spins phase will depend on the location of the nuclei (shown in Figure B1). As the gradient is applied the spins dephase and cause a periodic variation across the sample. This can be considered to have a frequency and is called the spatial frequency due to the gradient. As the gradient is applied for longer periods, the spins become more wound and the spatial frequency increases. If a sample is uniform, there will always be a magnetisation vector that cancels. However, in a periodic sample, the magnetisation does not cancel, and a signal can be detected (Figure B.3). Hence a spatial frequency of 0.5 mm^{-1} will produce a signal from periodic objects that have the periodicity of 1mm. This can be extended to two dimensions where the echo is sampled for different kx and ky spatial frequencies [56] [57].

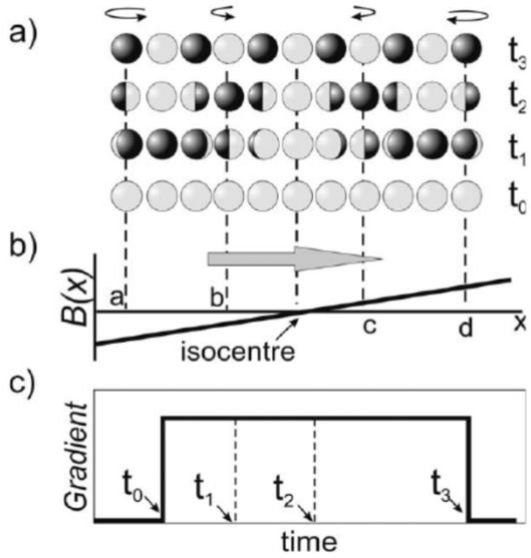

Figure B1. *The effect of a gradient field on the processing spins. a) Pictorial representation of the phases, b) The applied gradient field and c) Application of the gradient against time indicating times t_0,t_1,t_2 and t_3. Taken from* [57]

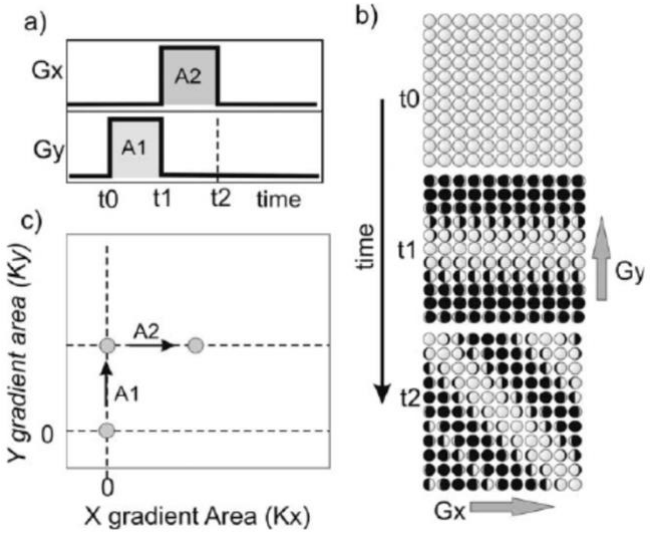

Figure B2. *The application of two gradients on the overall phases of the spin system. Taken from* [57].

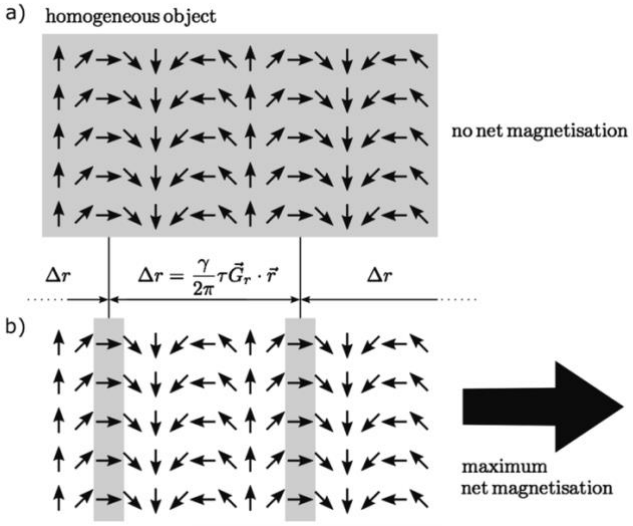

Figure B3. *The net magnetisation produced by a dephased sample showing how a spatial frequency produces a signal. Taken from* [56]

10.References

[1] I. Rabi, “A New Method of Measuring Nucelar Moment,” *Physical Review,* vol. 53, no. 4, pp. 318-318, 1938.

[2] S. Veeraraghavan, “NMR Spectroscopy and Its Value: A Primer,” *Journal of Chemical Education,* vol. 85, no. 4, pp. 537-539, 2008.

[3] A. R. Kherlopian, “A review of imaging techniques for systems biology,” *BMC Systems Biology,* vol. 2, no. 1, p. 74, 2008.

[4] M. Susan, “Nobel prize in medicine awarded to MRI pioneers,” *BMJ(Clinical Research ed.),* vol. 327, no. 7419, pp. 827-827, 2003.

[5] G. Sadigh, “Prevalence of Unanticipated Events Associated With MRI Examinations: A Benchmark for MRI Quality, Safety, and Patient Experience,” *Journal of the American College of Radiology,* vol. 14, no. 6, pp. 765-772, 2017.

[6] M. Mahesh, “The MRI Helium Crisis: Past and Future,” *Journal of the American College of Radiology,* vol. 13, no. 12, pp. 1536-1537, 2016.

[7] M. Zaitsev, “Motion artifacts in MRI: A complex problem with many partial solutions,” *Journal of Magnetic Resonance Imaging,* vol. 42, no. 4, pp. 887-901, 2015.

[8] C. B. Paschal, “K-space in the clinic,” *Journal of Magnetic Resonance Imaging,* vol. 19, no. 2, pp. 145-159, 2004.

[9] Y. Gossuin, “Physics of magnetic resonance imaging: from spin to pixel,” *Journal of Physics D: Applied Physics,* vol. 43, no. 21, p. 213001, 2010.

[10] J. S. Rigden, “Quantum states and precession: The two discoveries of NMR,” *Reviews of Modern Physics,* vol. 58, no. 2, pp. 433-448, 1986.

[11] B. M. Dale, MRI: Basic Principes and Applications, Chichester, West Sussex: Wiley-Blackwell, 2015.

[12] H. Rorschach, “A Classical Theory of NMR Relaxation Processes,” *Journal of Magnetic Resonance(1969),* vol. 67, no. 3, pp. 519-530, 1986.

[13] H. Günther, NMR Spectroscopy:Basic Principles, Concepts and Applications in Chemistry, John Wiley & Sons,Incorporated, 2013.

[14] F. Bloch, “Nuclear Induction,” *Physical Review,* vol. 70, no. 7-8, pp. 460-474, 1946.

[15] J. G. Webster, Webb's Physics Of Medical Imaging, Boca Raton , Florida: CRC Press, 2016, pp. 512-514.

[16] G. B. Chavhan, “Principles, Techniques, and Applications of T2*-based MR Imaging and Its Special Applications,” *RadioGraphics,* vol. 29, no. 5, pp. 1433-1449, 2009.

[17] E. Hahn, “Spin Echoes,” *Physical Review,* vol. 80, no. 4, pp. 580-594, 1950.

[18] H. Carr, “Effects of Diffusion on Free Precession in Nuclear Magnetic Resonance Experiments,” *Physical Review,* vol. 94, no. 3, pp. 630-638, 1954.

[19] R. Damadian, “Tumor Detection by Nuclear Magnetic Resonance,” *Science,* vol. 171, no. 3976, pp. 1151-1153, 1971.

[20] P. Lauterbur, “Image Formation by Induced Local Interactions:Examples Employing Nuclear Magnetic Resonance,” *Nature,* vol. 242, pp. 190-1, 1973.

[21] R. Damadian, “Field focusing n.m.r (FONAR) and the formation of chemical images in man,” *Philosophical Transactions of the Royal Society of London. B, Biological Sciences,* vol. 289, no. 1037, pp. 489-500, 1980.

[22] P. Mansfield, “Medical Imaging by NMR,” *The British Journal of Radiology,* vol. 50, no. 591, pp. 188-194, 1977.

[23] W. A. Edelstein, “Spin warp NMR imaging and applications to human whole-body imaging,” *Physics in Medicine and Biology,* vol. 25, no. 4, pp. 751-756, 1980.

[24] C. Westbrook, MRI at a glance, Wiley-Blackwell, 2015.

[25] R. Ansorge and M. Graves, The Physics and Mathematics of NMR, Morgan & Claypool Publishers, 2016, pp. 1-27.

[26] M. Stehling, “Echo-planar imaging: magnetic resonance imaging in a fraction of a second,” *Science,* vol. 254, no. 5028, pp. 43-50, 1991.

[27] C. M. Collins, Electromagnetics in Magnetic Resonance Imaging: Physical Principles, Related Applications, and Ongoing Developments, Morgan & Claypool Publishers, 2016.

[28] R. Mezrich, “A perspective on K-Space,” *Radiology,* vol. 195, no. 2, pp. 297-315, 1995.

[29] E. V. Reeth, “Super-resolution in magnetic resonance imaging: A review,” *Concepts in Magnetic Resonance Part A,* vol. 40A, no. 6, pp. 306-325, 2012.

[30] R. Pooley, “Fundamental Physics of MR Imaging,” *RadioGraphics,* vol. 25, no. 4, pp. 1087-1099, 2005.

[31] J. Hennig, “RARE Imaging: A fast imaging method for clinical MR,” *Magnetic Resonance in Medicine,* vol. 3, no. 6, pp. 823-833, 1986.

[32] M. Markl, “Gradient Echo Imaging,” *Journal of Magnetic Resonance Imaging,* vol. 35, no. 6, pp. 1274-1289, 2012.

[33] J. P. Ridgway, “Cardiovascular magnetic resonance physics for clinicians: part I,” *Journal of Cardiovascular Magnetic Resonance,* vol. 12, no. 1, 2010.

[34] A. Haase, “FLASH imaging.Rapid NMR imaging using low flip-angle pulses,” *Journal of Magnetic Resonance ,* vol. 67, no. 2, pp. 258-266, 1986.

[35] B. Hargreaves, “Rapid gradient-echo imaging,” *Journal of Magnetic Resonance Imaging,* vol. 36, no. 6, pp. 1300-1313, 2012.

[36] M. Poustchi-Amin, “Principles and Applications of Echo-planar Imaging: A Review for the General Radiologist,” *RadioGraphics,* vol. 21, no. 3, pp. 767-779, 2001.

[37] R. Rzedzian, “Real-time nuclear magnetic resonance clinical imaging in paediatrics,” *The Lancet,* vol. 322, no. 8362, pp. 1281-1282, 1983.

[38] R. L. DeLaPaz, “Echo-planar imaging,” *RadioGraphics,* vol. 14, no. 5, pp. 1045-1058, 1994.

[39] J. Tsao, “Ultrafast imaging: Principles, pitfalls, solutions, and applications,” *Journal of Magnetic Resonance Imaging,* vol. 32, no. 2, pp. 252-266, 2010.

[40] C. Ahn, “High-Speed Spiral-Scan Echo Planar NMR Imaging-I,” *IEEE Transactions on Medical Imaging,* vol. 5, no. 1, pp. 2-7, 1986.

[41] P. M. Jakob, “Basic pulse sequences for fast cardiac MR imaging,” *Basic pulse sequences for fast cardiac MR imaging,* vol. 6, no. 2-3, pp. 84-87, 1998.

[42] Y. Zhu, “Review: K-space trajectory development,” *IEEE 2013 International Conference on Medical Imaging Physics and Engineering,* pp. 356-360, 2013.

[43] D. A. Feinberg, “Halving MR imaging time by conjugation: demonstration at 3.5 kG,” *Radiology,* vol. 161, no. 2, pp. 527-531, 1986.

[44] R. C. Semelka, “HASTE MR Imaging: Description of Technique and Preliminary Results in the Abdomen,” *Journal of Magnetic Resonance Imaging,* vol. 6, no. 4, pp. 698-699, 1996.

[45] A. Deshmane, “Parallel MR imaging,” *Journal of Magnetic Resonance Imaging,* vol. 36, no. 1, pp. 55-72, 2012.

[46] M. Blaimer, “SMASH, SENSE, PILS, GRAPPA,” *Topics in Magnetic Resonance Imaging,* vol. 15, no. 4, pp. 223-236, 2004.

[47] D. J. Larkman, “Parallel magnetic resonance imaging,” *Physics in Medicine and Biology,* vol. 52, no. 7, pp. R15-R55, 2007.

[48] D. K. Sodickson, “Simultaneous acquisition of spatial harmonics (SMASH): Fast imaging with radiofrequency coil arrays,” *Magnetic Resonance in Medicine,* vol. 38, no. 4, pp. 591-603, 1997.

[49] K. P. Pruessmann, “SENSE: Sensitivity Encoding for Fast MRI,” *Magnetic Resonance in Medicine,* vol. 42, no. 5, pp. 952-962, 1999.

[50] L. Zhang, “HASTE sequence with parallel acquisition and T2 decay compensation: application to carotid artery imaging,” *Magnetic Resonance Imaging,* vol. 27, no. 1, pp. 13-22, 2009.

[51] T. Henzler, “Half-Fourier-Acquisition Single-Shot Turbo Spin- Echo (HASTE) MRI of the Lung at 3 Tesla Using Parallel Imaging With 32-Receiver Channel Technology,” *Journal of Magnetic Resonance Imaging,* vol. 30, no. 3, pp. 541-546, 2009.

[52] M. Uecker, “Real-time MRI at a resolution of 20ms,” *NMR in Biomedicine,* vol. 23, no. 8, pp. 986-994, 2010.

[53] C. M. Hyun, “Deep learning for undersampled MRI reconstruction,” *Physics in Medicine & Biology,* vol. 63, no. 13, p. 135007, 2018.

[54] R. Tongdee, “Utility of 3D magnetic resonance imaging in preoperative evaluation of hepatobiliary diseases,” *HPB,* vol. 8, no. 4, pp. 311-317, 2006.

[55] A. Nowogrodzki, “The world’s strongest MRI machines are pushing human imaging to new limits,” *Nature,* vol. 563, no. 7729, pp. 24-26, 2018.

[56] W. A. Worthoff, “CHAPTER 1:Introduction to Magnetic Resonance Imaging,” *Hybrid MR-PET Imaging: Systems, Methods and Applications,* pp. 1-44, 2018.

[57] D. Plewes, “Physics of MRI: A primer,” *Journal of Magnetic Resonance Imaging,* vol. 35, no. 5, pp. 1038-1054, 2012.

[58] M.Stehling, “Echo-planar imaging: magnetic resonance imaging in a fraction of a second,” *Science,* vol. 254, no. 5028, pp. 43-50, 1991.

[59] S. Currie, “Understanding MRI: basic MR physics for physicians,” *Postgraduate Medical Journal,* vol. 89, no. 1050, pp. 209-223, 2012.

[60] B. Jung, “Spin Echo Magnetic Resonance Imaging,” *Journal of Magnetic Resonance Imaging,* vol. 37, no. 4, pp. 805-817, 2013.